

Can climate patterns predict dengue outbreaks? A causal-based analysis on the role of climate change in *Aedes*-borne disease transmission

Javier Corvillo^{1, 2*}, Verónica Torralba^{2*}, Diego Campos², Ana Rivière-Cinnamond³, and Ángel G. Muñoz¹

¹Complutense University of Madrid, Department of Earth Science and Astrophysics, Madrid, 28040, Spain

²Barcelona Supercomputing Center, Earth Sciences Department, 08034, Spain

³Pan-American Health Organization, Communicable Diseases and Health Analysis, Panama City, 0843-03441, Panama

*javier.corvillo@bsc.es / veronica.torralba@bsc.es / angel.g.munoz@bsc.es

ABSTRACT

Background: Vector-borne diseases transmitted by *Aedes* mosquitoes such as dengue, Zika, and chikungunya, pose significant public health challenges worldwide in the wake of human-driven climate change. However, while their transmission is known to be susceptible to some climate variables like temperature or the amount of rainfall, the overall role of climate patterns on the emergence of these diseases is not so well understood.

Methods: Using data from a number of sources, we explore and analyse the response of *Aedes*-borne disease transmission to climate patterns, in order to understand its influence on disease outbreaks. Our analysis is composed of three different studies: 1) a timescale decomposition of disease transmissibility values, thereby guiding officials to understand the behaviour of outbreaks for budget and resource allocation; 2) a correlation analysis between transmissibility values and different climate patterns, such as El Niño Southern Oscillation, in order to understand the effects of natural climate patterns onto *Aedes*-borne outbreaks; and 3) a causality analysis to solidify findings obtained through correlation, identifying the most relevant predictors and their applicability in a climate-and-health service framework for forecasting the transmissibility of *Aedes*-borne diseases.

Results: (Fill up after 1st draft is done)

Conclusions: (Fill up after 1st draft is done)

Keywords: Public Health, Vector-borne Diseases, Epidemiology, Climate Change, Climate Services, Environmental Sciences

1 Multilingual abstracts

Please consult the [Additional files](#) section for abstract translations into the other five official languages of the United Nations (Arabic, Chinese, French, Russian and Spanish).

2 Background

2.1 The emergence of vector-borne diseases in the context of climate change

Disease stability and transmissibility under changing climate conditions has long been a topic of interest and research in the fields of epidemiology and virology. Many viral, bacterial, and parasitic diseases have been shown to be susceptible to changes in environmental conditions across different regions and timescales^{1,2}. This is particularly true for previously pandemic diseases that have become endemic once proper disease control mechanisms are implemented by public health officials³. Prevalent respiratory viruses such as H1N1 influenza or the novel SARS-CoV-2 virus

have been shown to reduce their dependency on human spread once losing their pandemic status, adopting defined climate-dependent seasonality patterns and becoming more prominent in temperate climates during the winter season^{4,5}.

For vector-borne diseases (VBDs), the relationship between climate and pathogen transmissibility is even more intertwined. Carriers such as arthropods, snails and slugs thrive under specific climate-dependent thresholds and conditions, and in the context of anthropogenic climate change, the effects of global warming and changing precipitation patterns have been shown to affect the distribution and behaviour of these vectors^{6,7}.

Mosquitoes of the *Aedes* genus, such as *Aedes albopictus* and *Aedes aegypti*, are of particular interest and importance in medium and low income countries⁸. As the main carriers of diseases like dengue (DENV), chikungunya (CHIKV), and Zika (ZIKV), they pose a significant public health threat,

traditionally in tropical and subtropical regions⁹. In the Americas, for instance, DENV impacts account for over 2 million disability adjusted life years worldwide¹⁰, and a low estimated annual cost of about US\$2.1 billion¹¹.

However, the effects of climate change are causing *Aedes*-related diseases not only to emerge in new, previously unaffected regions, but also to increase their spread in areas where they were previously endemic¹². Along with compounded changes in urbanization¹³ and population growth¹⁴, climate change is believed to be a major driver of increased DENV incidence in temperate climates¹⁵, with the recent establishment of epidemic activity in parts of North America¹⁶ or Southeast Asia¹⁷, and detection of local transmission in southern European countries along the Mediterranean Basin¹⁸. Equatorial tropical and subtropical zones like the Sub-Saharan Africa, Southeast Asia, and northern South America have also been subject to higher incidence over the past 40 years¹⁹. While the current yearly incidence of DENV amounts to an average of 400 million cases per year²⁰, it is believed that the effects of climate change may put an additional 2.5 billion people at risk of DENV if *Aedes* vectors were present in every region where the climate is suitable for their development¹⁹.

2.2 Known drivers on *Aedes*-borne disease transmission dynamics and their impact

The current scientific literature highlights a profound influence of the environmental conditions over *Aedes* mosquito proliferation, with temperature and precipitation being the two primary climate drivers of *Aedes*-borne disease transmission due to their impact on both vector and pathogen biology alike.

Many vector physiological processes (e.g., biting frequency, reproduction rates) as well as pathogen characteristics (e.g., extrinsic incubation duration) are conditioned by temperature, increasing until certain temperature thresholds are reached²¹. In a similar manner, rainfall promotes the availability of mosquito breeding sites up until a critical point, in which excessive rainfall may flooding or washing out the mosquito larvae away²². In conjunction, the combined effects of temperature and rainfall play a crucial role in the length of the *Aedes*-borne transmission season of DENV, CHIKV and ZIKV in temperate areas and affected hotspots, with higher incidence particularly in urban areas of the Western Pacific and the Eastern Mediterranean regions²³.

Aside from these climate variables, humidity is also another probable factor in the proliferation of *Aedes* mosquito breeding sites, though proper characterization and relationships with disease transmission remains an object of study. Current evidence suggests that elevated humidity levels could play a role in reducing incubation periods and blood-feeding cycle duration in *Aedes* mosquitoes²⁴.

2.3 Climate patterns as an aggregate of unknown transmissibility drivers

While the aforementioned macro climatic factors have been widely used in *Aedes*-borne disease research and modelling^{25–28}, it is widely acknowledged that these are not enough to fully explain the climate component of *Aedes*-borne disease transmissibility, and that more explanatory variables can aid in building more refined and actionable DENV monitoring and prediction systems^{29–32}. For instance, temperature and rainfall may also affect other possible small-scale climate modulators like soil moisture or vegetation growth, which in turn may affect the availability of breeding sites for *Aedes* mosquitoes. Additionally, analysis of high resolution satellite imagery has suggested that land cover change, through deforestation, as well as stagnant water bodies, may also play a role in the proliferation of *Aedes* breeding sites³³.

From a pragmatic perspective, understanding the contribution of each of these additional climate variables, each operating in different spatial and temporal scales, can be a challenging undertaking. Many of these variables lack comprehensive long-term observational records, particularly in tropical and southern regions where *Aedes* diseases are most prevalent^{34,35}. Moreover, computational constraints may arise when attempting to model multiple interacting variables simultaneously, and the sheer number of potential variables makes it difficult to determine which combinations are most relevant for disease prediction without extensive computational resources. Moreover, the effects of these variables may not be immediately apparent, as variables like soil moisture, for instance, do depend on many sub-processes³⁶.

It is for this reason why climate patterns, in this context, may serve a better role in understanding the underlying climate processes behind *Aedes*-borne disease transmission. Climate patterns are large-scale recurring ocean or atmospheric phenomena that can influence weather and climate conditions over different timescales (subseasonal, seasonal, inter-annual, decadal, etc.). They are often characterized by their periodicity, identified through their defined climate variability indices, and their effects ripple through the climate system, affecting temperature, precipitation, and other climate variables across different regions through teleconnections³⁷.

As such, climate patterns may serve as aggregators of both large and small climate phenomena by linking various climatic oscillations to regional weather events and other environmental processes³⁸. The analysis of known seasonal patterns such as the El Niño Southern Oscillation (ENSO) could provide a framework for understanding complex interactions that influence precipitation, temperature, and ultimately, the role of these compound climate variables processes on *Aedes*-disease transmission. Moreover, since they encapsulate broader climatic trends that affect local conditions, climate patterns seem preferable over everyday climate variables

in the development of future climate-and-health *Aedes* prediction systems^{39,40}.

2.4 The applicability of climate services in vector-borne disease prevention

Given the worldwide impacts of DENV, ZIKV and CHIKV and their expected potential to spread to unprepared regions, the need for effective *Aedes*-borne disease control is more pressing than ever. To this end, many climate-and-health initiatives have been developed in recent years, with the aim of providing actionable information to public health officials and decision-makers, such as the Tropical Disease Research initiative from the World Health Organization's (WHO)^{41,42}, as well as its Global Strategic Preparedness, Readiness and Response Plan, with \$55 million in funding from different stakeholders and public officials. Other examples include the mapping of environmental suitability for DENV, ZIKV and CHIKV^{43,44}, or the development of integrated surveillance systems for *Aedes* arboviruses⁴⁵.

The development of early warning systems (EWS) for *Aedes* vectors are also another area of focus in which climate information may translate to more actionable health information⁴⁶. While disease EWS can be based on clinical and epidemiological data alone, the integration of climate information at different timescales (subseasonal, seasonal, inter-annual, decadal) can improve the accuracy and skill of these systems while simultaneously extend the window over which changes in transmissibility can be detected^{47,48}.

Here, we aim to characterise the behaviour and climatology of the climate-driven component of *Aedes*-borne transmissibility, in order to understand its evolution overtime in the context of climate change, but also to understand how the different climate timescales may influence the possibility of outbreaks in different regions and seasons. Additionally, we aim to understand the role of climate patterns in the predictability of *Aedes*-borne disease outbreaks, in order to establish their relevance for operational vector-borne disease control, and to highlight which climate patterns may be used as predictors under a possible causal-based outbreak prediction system.

3 Methods

We utilize a select number of datasets and methodologies to undertake three distinct analyses, in order to characterise the behaviour of the climate component of *Aedes*-borne disease transmissibility, and to understand the role of climate patterns in their potential predictability.

By using global climate products that transform climate variables into the climate-driven component of *Aedes*-borne transmissibility, we can explore its underlying mechanisms over affected and emerging areas at multiple timescales (seasonal, inter-annual, decadal, and long-term

trends). We later employ a series of correlation and causality analyses in order to understand the role of climate patterns on *Aedes*-disease emergence across regions and seasons. By highlighting which climate patterns are dominant over the different areas and seasons, we can assess their impact on the transmissibility of *Aedes*-borne diseases, therefore determining whether they may qualify as predictors for future DENV, ZIKV or CHIKV outbreaks.

3.1 R_0 as a bridge between climate and health

In recent years, at least three main mechanisms have been discussed to explain the seasonality of VBDs⁴⁹: the effects of the vector's behaviour (e.g. absence or presence in the area), human behaviour (e.g. whether an infected host can transmit the disease by travelling), and the climate (whether the conditions are favourable for the vector to transmit the disease). These three mechanisms are usually encapsulated in the basic reproduction number, or R_0 , which is a commonly used epidemiological metric that quantifies the transmissibility of vector-borne diseases, and is defined as the average number of secondary cases generated by a single infected individual in a susceptible population⁵⁰.

However, while R_0 entangles vector, human, and climate behaviour, by only integrating the climate component of the disease transmission for the computation of R_0 , then the resulting R_0 metric is more so interpreted as the role of environmental conditions in the spread of the disease. Thus, this definition of R_0 , which we can understand as the diseases' environmental suitability, can be understood as a first approximation of the role of the climate in the dynamics of vector-borne diseases. This tweaked definition of R_0 is one of the operational outbreak indices used by WHO, along with several other decision-making institutes and health practitioners in disease control and prevention^{51,52}.

3.2 The *Aedes* Disease Environmental Suitability 2's monitoring system

The *Aedes* Disease Environmental Suitability 2's (AeDES2) monitoring system⁴⁴ was used throughout this study in order to obtain the R_0 values for the analysis. Improving over its predecessor⁴³, AeDES2 is a climate-and-health service that provides real-time monitoring of the environmental suitability for *Aedes*-borne diseases. The system uses a climate variables like temperature and precipitation, and through its integration with ento-epidemiological models, as well as with calibration with recorded DENV cases, R_0 values are computed for different regions and seasons. The monitoring system is designed to be used by public health officials and researchers to assess the risk of disease outbreaks and to inform prevention and control strategies.

In this context, our analysis is then composed of three different studies:

Index Name	Abbreviation	Periodicity	Pattern Type
Atlantic 3 Index	ATL3	Several months to a few years	Oceanic
Indian Ocean Basin	IOB	Several months to a few years	Oceanic
Indian Ocean Dipole	IOD	Between 2-7 years	Oceanic
El Niño 3.4 Index	Niño 3.4	Between 2-7 years	Oceanic
North Pacific Meridional Mode	NPMM	Several months to a few years	Atmospheric
South Atlantic Subtropical Dipole	SASD	Several months to a few years	Oceanic
Southern Indian Ocean Dipole	SIOD	Several months to a few years	Oceanic
South Pacific Meridional Mode	SPMM	Several months to a few years	Atmospheric
Tropical North Atlantic	TNA	Several months to a few years	Oceanic

Table 1. Summary of the climate variability indices used in the analysis used for the correlation and causality studies.

3.3 Analysis 1: Multi-timescale climate decomposition of R_0

With the intent of isolating the signal of man-made climate change from the natural variability R_0 data, a timescale decomposition methodology was used to obtain the total variance across different timescales. This approach allows us to separate the complex R_0 signal into several temporal components, each providing insight into the underlying climatology of *Aedes*-borne disease transmission. This decomposition is particularly useful for health-officials in historically affected DENV hotspots, where understanding how different climate processes condition disease transmissibility at various temporal scales is essential for the development of effective public health strategies, optimization of resource allocation, or implementation of targeted intervention strategies through the use of early warning systems for disease outbreak prevention^{53,54}.

3.3.1 Data

The timescale decomposition analysis was undertaken using R_0 outputs from the AeDES2's monitoring system. The 1951-2024 monthly-mean period of AeDES2's R_0 values was selected for the analysis, for a total of 888 months or 295 full seasons. Considering that vector borne diseases are extending to previously unaffected areas due to the effects of man-made climate change, AeDES2's coverage has been increased since its inception to contain global outputs, allowing for a comprehensive analysis of the relationship between climate variability indices and R_0 both in current *Aedes* hotspots and emerging regions.

3.3.2 Methodology

As R_0 doesn't follow a clearly defined probability distribution function, the temporal analysis filters a given R_0 time-series of any given grid-point by employing the non-parametric locally estimated scatterplot smoothing technique (LOESS)⁵⁵. Sensitivity tests have been conducted in order to obtain the best LOESS smoothing parameter for the analysis, selecting the value that provides the lowest Generalized Correlated Cross-Validation (GCV) verification metric for the goodness of fit of the model⁵⁶. GCV provides a robust assessment of model generalizability by directly penalizing overfitting through its leave-one-out validation procedure⁵⁷.

Once the ideal LOESS smoothing parameter is found for the R_0 data, the R_0 time-series for each grid-point is separated into four components: a long-term trend signal (understood to be the trend caused by anthropogenic climate change), an inter-annual signal (year to year), a decadal signal (10-30 years), and lastly, a remainder signal which contains other signals of the data (i.e., inter-annual and inter-decadal variability, among others). Variance maps for each of these four components capture the overall direction of the data over time, as well as the climatological variability of R_0 in any given grid-point. Variance maps, as well as any results from following analyses, are shown for global outputs.

After the variance maps are obtained, R_0 values are then detrended for the following correlation and causality analyses. While detrending through the assumption that R_0 changes linearly over time could be a valid approach, it fails to capture the temperature dependency of the data. In order to account for this intrinsic relationship of R_0 with temperature, a similar timescale decomposition analysis is performed on the detrended R_0 data, but using temperature data from the AeDES2's monitoring system datasets as the independent variable (monthly-mean temperature data consisting of the GHCN-CAMS project⁵⁸, the CPC Unified Global Temperature dataset⁵⁹, and the ERA5 and the ERA5Land reanalysis datasets⁶⁰). In this way, the obtained trend serves as a functional relationship between temperature and R_0 : a temperature-based description of the R_0 signal, attributed to the warming of the planet⁶¹.

3.4 Analysis 2: Correlation studies between R_0 and climate variability indices

After analyzing the R_0 signal and its variability through timescale decomposition, we assess the impact of several climate variability indices on global R_0 values over the chosen 1951-2024 monthly-mean period.

3.4.1 Data

Correlation studies are performed over global outputs, using the temperature-based detrended R_0 data as in the previous analysis over the different seasons. A total of 9 temperature-based climate variability indices have been used for the cor-

relation analysis, which have been computed using the detrended temperature data utilized in the previous analysis. Their periodicity, as well as their main pattern type, are listed and summarized in Table 1.

3.4.2 Methodology

The correlation analysis was performed using the Spearman correlation coefficient, assesses how well an arbitrary monotonic function can describe the relationship between two variables⁶². For computation of statistical significance in correlation, the non-parametric Monte Carlo method was used⁶³, with a p-value threshold of 0.05.

3.5 Analysis 3: Causality studies between R_0 and climate variability indices. Outlining of predictors for disease outbreaks

Causal-based patterns can be identified after this analysis, which allow for a more robust foundation for the understanding of the underlying mechanisms between climate variability and R_0 patterns. These causality studies are performed over global outputs and over the different seasons. Along with results obtained through correlation, this causality analysis can be used to outline the most relevant predictors for disease outbreaks. These predictors, in turn, can be used for the refining and building of AeDES2's prediction system for improving the accuracy and skill of the ensemble forecasts compared to its predecessor.

3.5.1 Data

The datasets that were used for the causality analysis are the same detrended datasets as those employed in Section 3.4.1.

3.5.2 Methodology

Causality analyses between R_0 and climate variability indices were performed by using Liang-Kleeman's proposed methodology for computing information flow between two entities of a dynamical system, quantifying the amount of information that one time series (the climate variability indices) can provide about another time series (R_0 patterns)⁶⁴. Once the transfer entropy is computed, it is then normalized in order to account for the different scales of the two time series⁶⁵. Statistical significance is computed using Fisher's information matrix, with a p-value threshold of 0.05.

4 Results

The most relevant results from each of the three analyses are summarized over the following sections of the manuscript, highlighting the most relevant findings and their implications. The complete results from the analyses described above, including the correlation and causality study maps for each individual climate pattern over the different seasons, can all be found in the supplementary material provided along with this manuscript (see [Additional files](#)).

4.1 Analysis 1: Multi-timescale climate decomposition of R_0

The resulting timescale decomposition maps for R_0 global outputs for the whole time series can be found in Figure 1, along with the component time series for the cities of Iquitos, Peru, known to be a traditional hotspot of *Aedes*-borne diseases, and Santa Fe, Argentina. The optimal span values of LOESS smoothing for the timescale decomposition methodology for this sample period was found to be 8 months for the GCV verification metric. It is worth noting that, because the R_0 metric operates in certain temperature ranges, grid points with less than 6 months of data per year were excluded from the analysis, in order to prevent poor seasonal component estimation due to missing entire seasons.

Over the 74-year period, the long-term trends and residual components of R_0 (Figures 1a and 1d) show the highest variance contribution in tropical and subtropical regions, particularly across central Africa, parts of South America including the Amazon basin, and scattered areas in Southeast Asia and northern Australia (the sum of these components rounding between 40-80%). These trend patterns suggest that long-term climate change, along with interannual climate variability, is driving systematic shifts in R_0 in these traditionally endemic regions, reflecting the complex interactions between temperature, humidity, and precipitation influencing vector populations and virus transmission. For these regions, there is no clearly defined transmission season over the year, as the seasonal signal of R_0 (Figure 1b and 1e) is rather poor. Instead, the climatology of R_0 in these regions, due to the high temperature and humidity values, adopts high R_0 values which remain constant throughout the year, independently of the season.

Though the decadal component (Figure 1c) shows a nigh negligible contribution across all regions of the globe, the seasonal variance (<5%, Figure 1b) shows a markedly different geographical distribution, with the highest contributions (between 60-100% variance explained) concentrated in regions with pronounced seasonal temperature variations. Notable hotspots include the northern edges of traditional dengue transmission zones in South America, parts of southern Africa, central Asia, and importantly, temperate regions that border current endemic areas. It is in these regions where the seasonal temperature fluctuations strongly condition the transmissibility season of R_0 , reaching its peak around the summer months.

Indeed, Figure 1f highlights the effect of the seasonal component on the overall R_0 dynamics in these strong seasonal regions. While the trend component accounts for a significant portion of the variance, it is the seasonal component that can play a crucial role in defining whether a DENV outbreak can occur ($R_0 > 1$) or not ($R_0 < 1$).

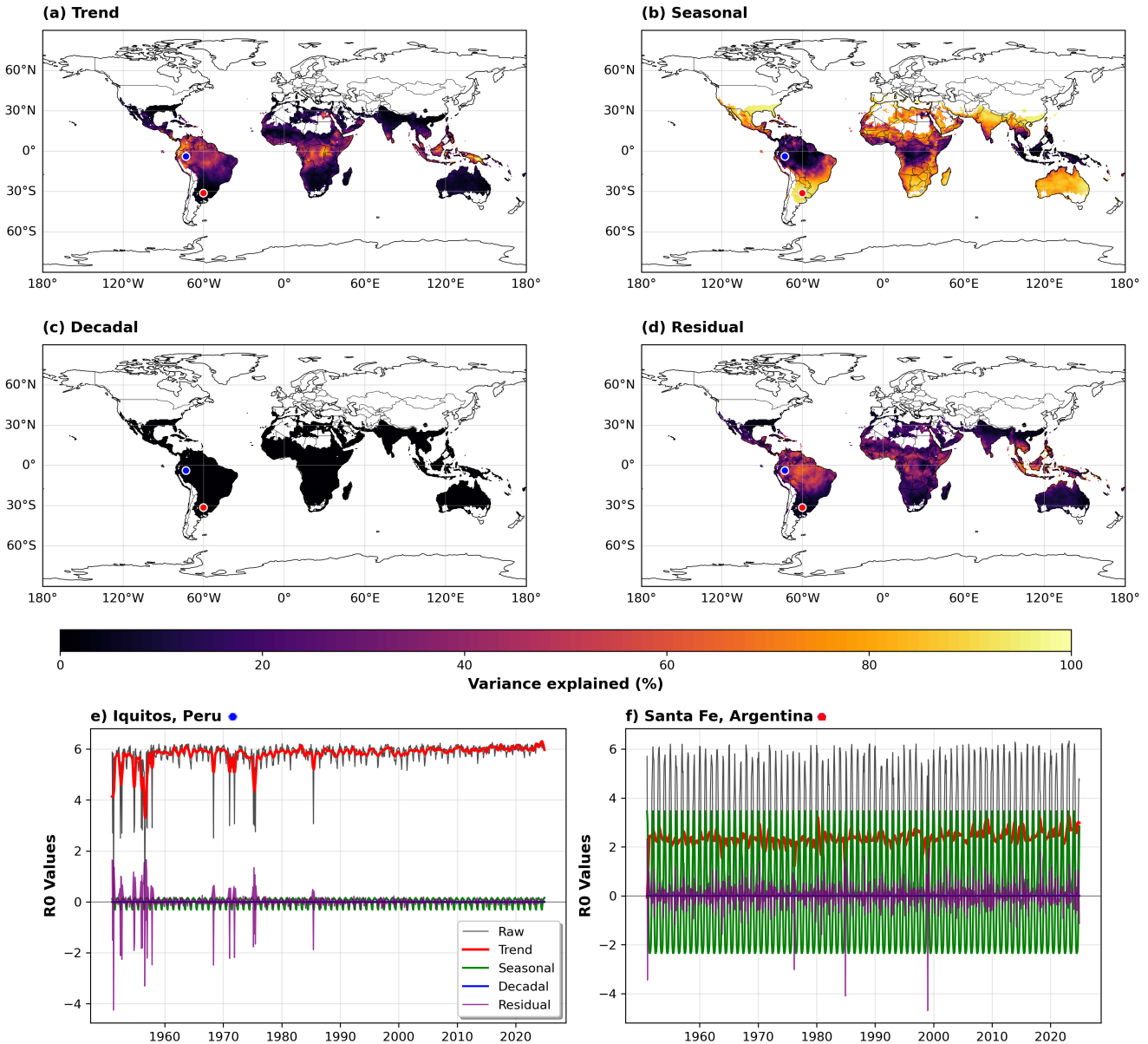


Figure 1. a-d) Global timescale decomposition maps for R_0 values for the monthly mean 1951-2024 period, different components. The time series for the cities of Iquitos, Peru (blue dot), and Santa Fe, Argentina (red dot), are shown as examples in e) and f) respectively.

Two subsets of the seasonal variance results, corresponding to the 1961-1990 and 1991-2020 climatologies, can be found in Figure 2, along with their respective Köppen-Geiger climate classification maps⁶⁶. For these two periods, the GCV-optimal span value of LOESS smoothing is also 8 months, same as for the complete time series.

When examining the variance patterns in relation to the Köppen-Geiger classification, distinct climate zone signatures can become apparent on a first-approximation basis. Tropical climate zones (A-type climates in the Amazon basin, central Africa, and Southeast Asia) demonstrate

characteristic patterns where trend and residual variance typically dominates. Alternatively, temperate and humid subtropical zones (C-type climates in southern Brazil, parts of East Asia, and the Mediterranean basin) show a more pronounced seasonal component. At a glance, it may seem that a study on the expansion of A and C type Köppen Geiger climates in the context of climate change may provide a useful framework for predicting the evolution of *Aedes*-borne transmissibility, with each major climate type exhibiting distinct characteristics that condition the R_0 signal.

However, this would be a naive approach, since the

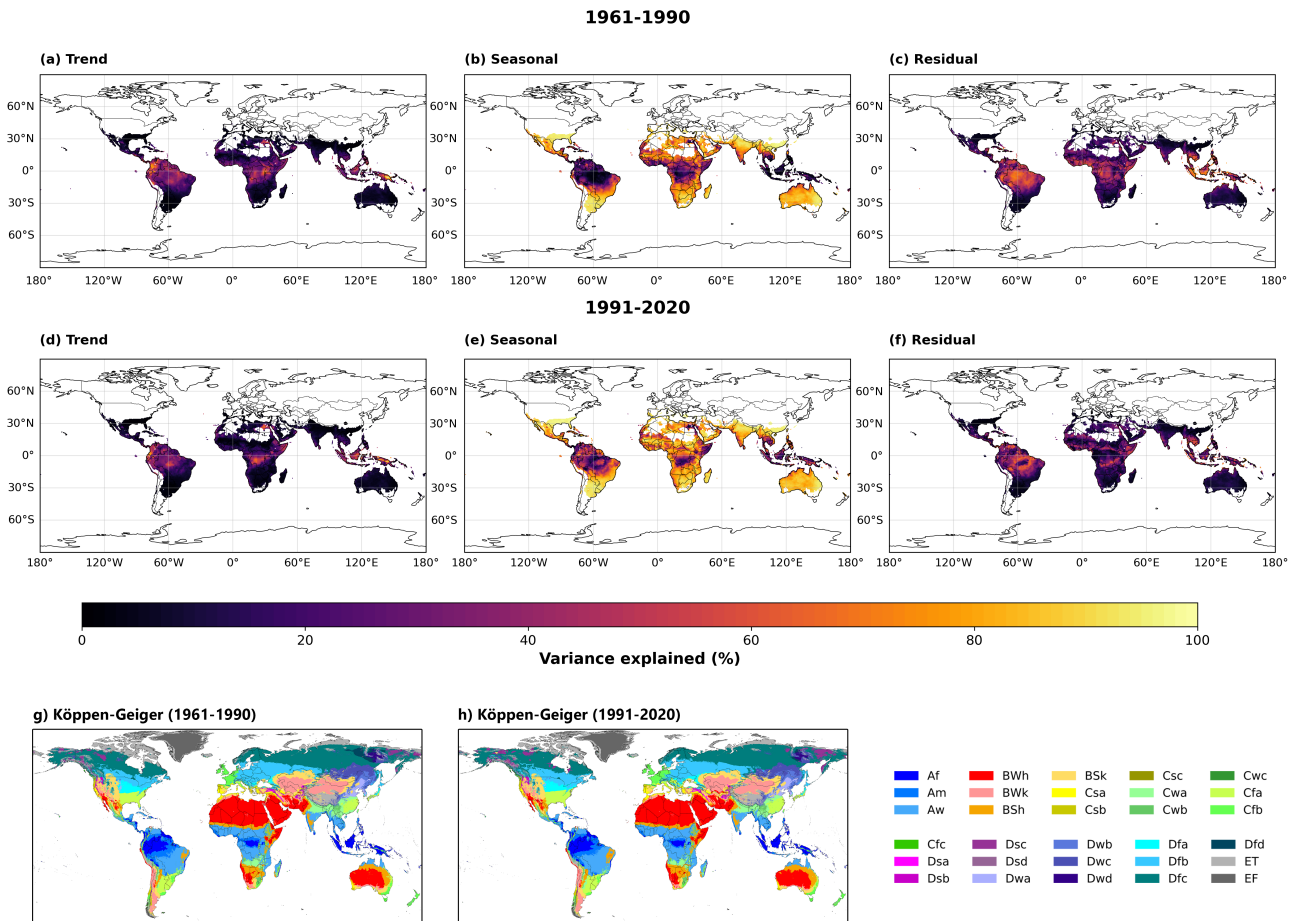


Figure 2. a)-c) Global timescale decomposition maps for R_0 values for the monthly mean 1961-1990 period, different components. Its associated Köppen-Geiger climate classification is shown in g). d)-f) Global timescale decomposition maps for R_0 values for the monthly mean 1991-2020 period, different components. Its associated Köppen-Geiger climate classification is shown in h). (Source for Köppen-Geiger climate classification maps:⁶⁶)

Köppen-Geiger classification is a static classification system that does not thoroughly reflect the dynamic nature of climate change⁶⁷. Indeed, the comparison between the two 30-year periods reveals notable shifts in how climate variability affects R_0 across different regions. In the 1961-1990 period, the trend component shows more concentrated high-variance zones, particularly in central Africa and tropical parts of South America. By the later 1991-2020 period, these trend patterns have intensified in some regions while diminishing in others, highlighting that the impacts of systematic climate change on transmission potential, while shown to have become more pronounced over time, are not entirely straightforward.

Given the strong seasonality of R_0 in temperate regions through these timescale decomposition analyses, and given the different climate variables that *Aedes*-borne transmissibility seems to relate to besides temperature, it is not unreasonable to expect R_0 values to be closely related to

seasonal, temperature-driven climate patterns, be it in the form of correlation or causality. The following analyses aim to explore these relationships further, with the climate variability indices previously listed in Table 1.

4.2 Analysis 2: Correlation studies between R_0 and climate variability indices

Spearman correlation outputs between R_0 and the El Niño 3.4 index for all seasons of the time series are shown in Figure 3. The same study has been reproduced for all other climate variability indices, and its respective results can be found in the supplementary material.

The most consistent positive correlations across seasons appear in the Amazon basin and northeastern South America, tropical A-type climate regions in the Köppen Geiger classification that correspond to areas of high trend and residual variance in the previous timescale analyses of section

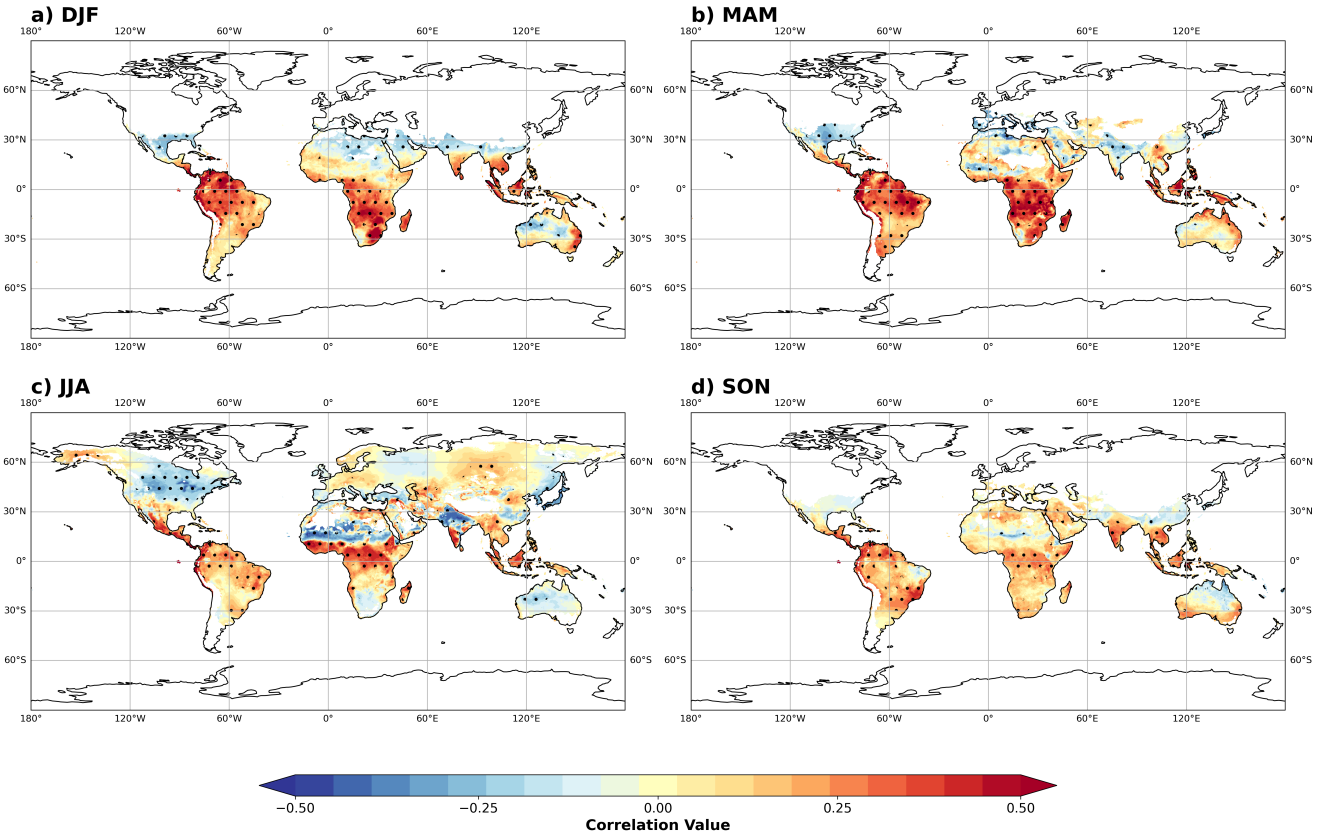


Figure 3. a)-d) Correlation values between R_0 and the Niño 3.4 index, for the 1951-2024 monthly mean period in all seasons. Dots represent statistically significant correlation values, at $p < 0.01$.

4.1. The austral summer and autumn seasons (figures 3a and 3b) show the highest positive correlation values in those regions, with Africa exhibiting more heterogeneous patterns with both positive and negative correlation zones in the austral autumn. It is during these months that we also observe notable emergence of negative correlations in parts of Southeast Asia, along with the appearance of positive correlations in some temperate transition areas as well.

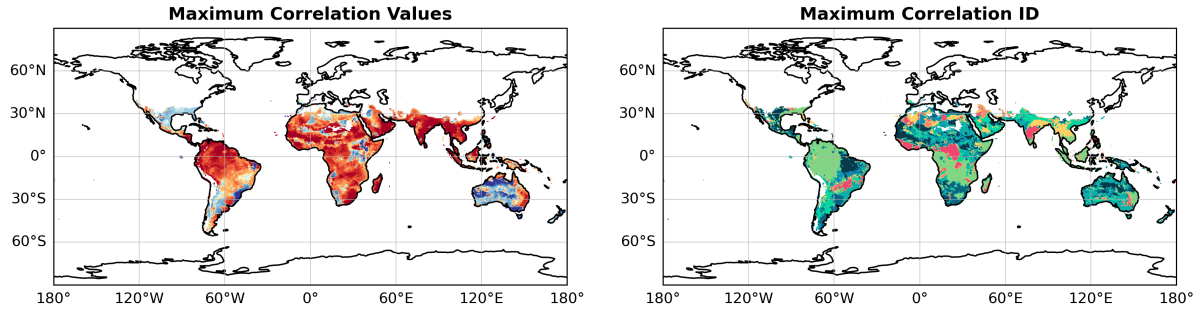
Over the austral winter (Figure 3c), the correlation patterns shift overall in the Southern Hemisphere. Fewer regions, with Africa in particular, show predominantly weaker correlation values. Negative correlations additionally emerge over the Sahel region, India and the East Coast of the United States. The austral spring (Figure 3d) demonstrates a return to stronger correlation patterns, particularly in South America where positive correlations re-intensify across the Amazon and southern Brazil regions.

An aggregate of the maximum statistically significant correlation values between R_0 and all climate variability indices, as well as the index that gives the maximum correlation value, is shown in Figure 4. The left column shows the maximum correlation values for each index, while

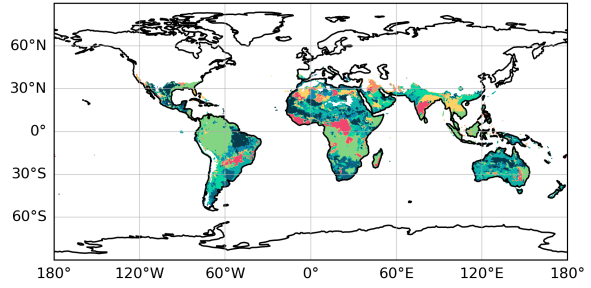
the right column shows which index gives the maximum correlation value for each grid point. The percentage of grid points over which each index gives the highest statistically significant correlation values is shown in Figure 5. It is worth noting that, since the difference between correlation values can often be small, the second and third highest correlation values are also shown in the figure, in order to provide a more complete picture of the relative importance of each index.

Over the austral summer and autumn months (Figure 4a-b) the El Niño 3.4 index is the most dominant index in the regions previously highlighted in Figure 3a-b. However, as the El Niño 3.4 correlation with R_0 weakens during the austral winter and spring months over its zones of influence (Figure 3c-d), other climate indices are vying for dominance in its stead (Figure 4c-d, right). This behavior is also replicated in the regions of more seasonal R_0 variance described in section 4.1, where the spread of the indices over which maximum correlation is attributed to becomes more heterogeneous (Figure 4a-d, right). Notable areas include the Sahel region, Mediterranean basin, parts of southern Africa, Australia, the East Coast of the United States and southeastern Asia, where different indices dominate the correlation landscape depending on the season.

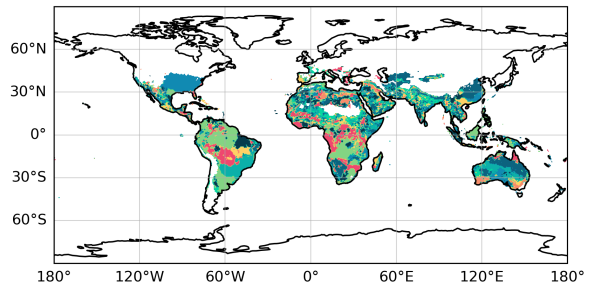
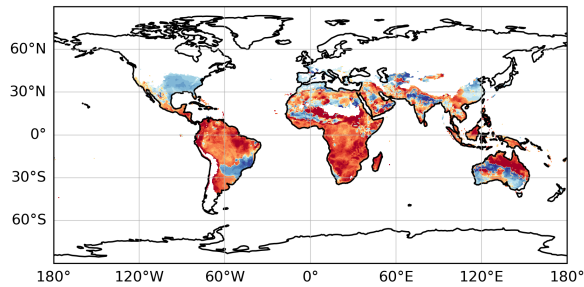
a) DJF



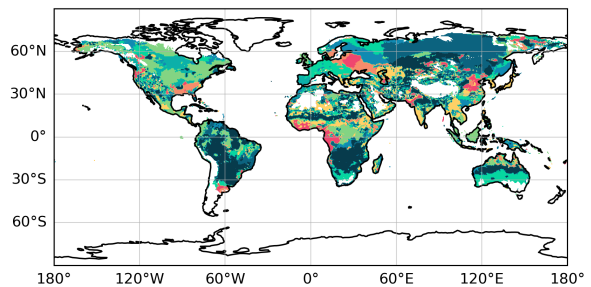
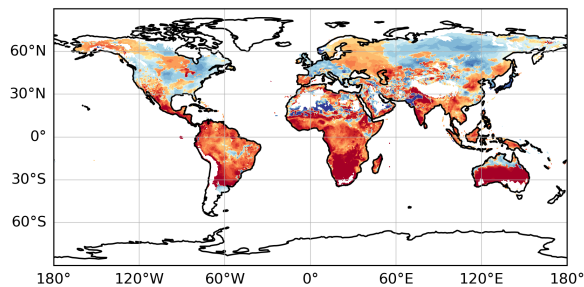
Maximum Correlation ID



b) MAM



c) JJA



d) SON

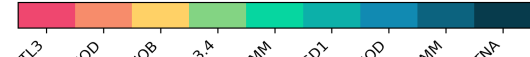
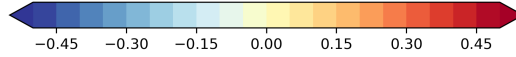
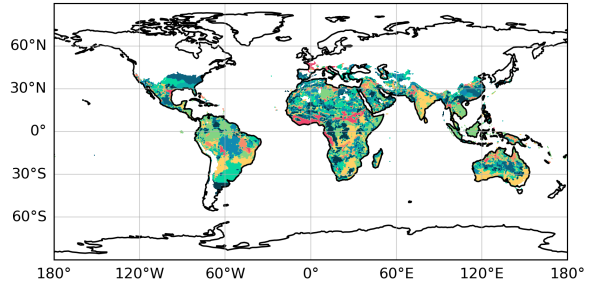
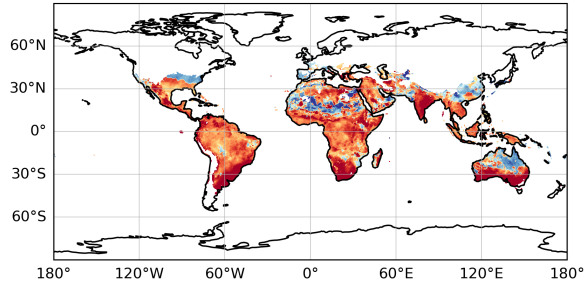


Figure 4. a-d) For all seasons: Left, maximum statistically significant correlation values between R_0 and all indexes of Table 1, for the 1951-2024 monthly mean period ($p < 0.01$). Right, which climate index gives the maximum statistically significant correlation values.

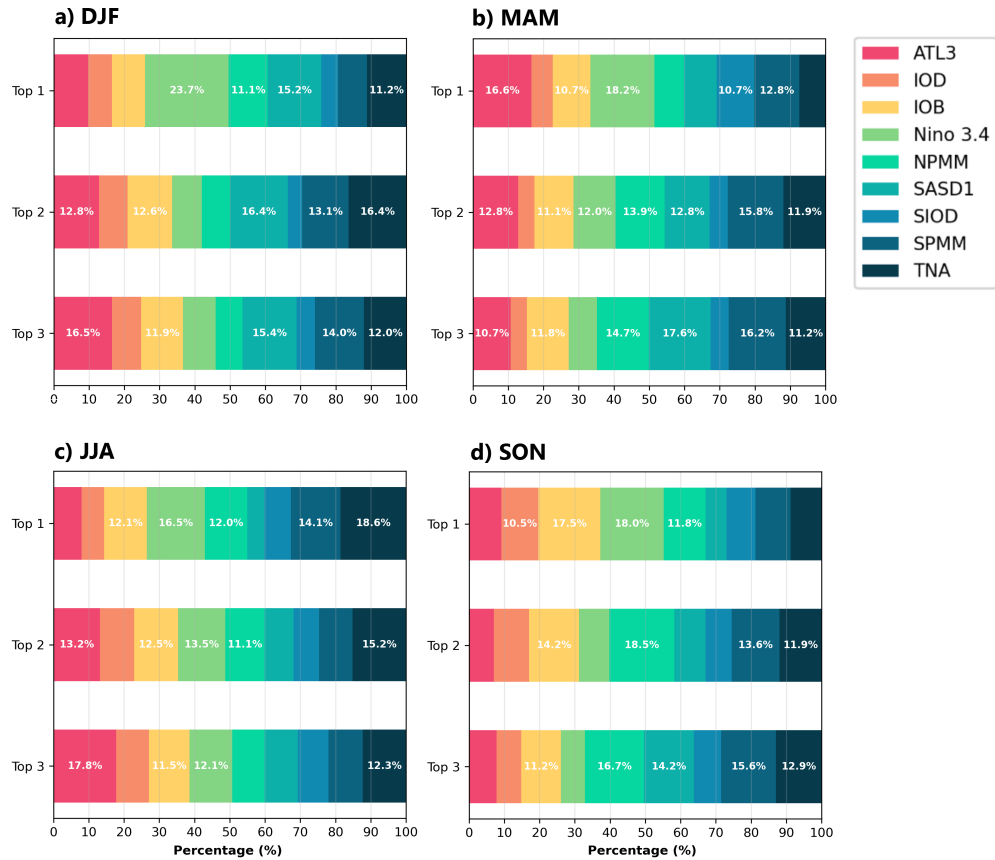


Figure 5. a)-d) For all seasons: Percentage of grid points over which each index gives the highest, second or third highest statistically significant correlation values. Any contribution above 10% is labeled in the barplots.

With this, it is soon evident that multiple seasonal temperature-based climate indices compete for dominance across different regions and seasons, with no single index controlling more than 25% of grid points as the primary correlate, in accordance to Figure 5. Still, other notable indices include the IOB index, contributing more than 10% of grid points in nearly all categories and being prevalent in India during the austral winter and spring months. These findings and results for both El Niño and IOB are consistent with previous studies that have highlighted the importance of both climate patterns in influencing climate variability and its potential impact on *Aedes*-borne disease transmission^{68–70}.

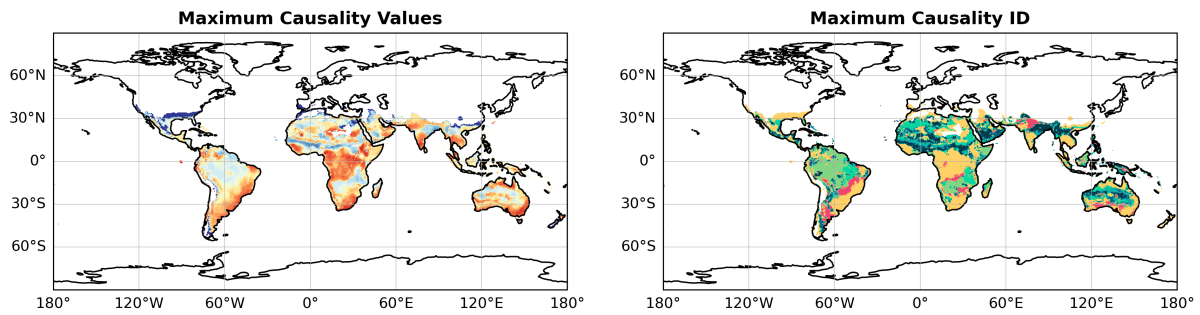
Despite their respective contributions however, the spread of all nine indices is relatively even, with no single index clearly dictating whether R_0 is directly tied to one specific climate pattern, reflecting the multifaceted nature of climate variability influence on *Aedes*-borne disease transmission.

4.3 Analysis 3: Causality studies between R_0 and climate variability indices. Outlining of predictors for disease outbreaks

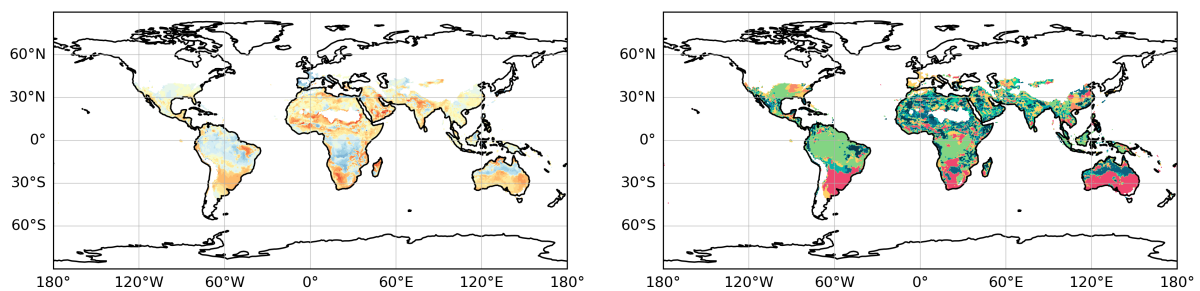
Analogues of figures 4 and 5 for section 4.3 are shown in Figures 6 and 7 for the Liang-Kleeman causality analysis. The causality analysis is performed over the same 1951-2024 monthly mean period, with the same climate variability indices of Table 1.

As opposed to the correlation outputs in Figure 4, the causality analyses in Figure 6 show a pronounced attenuation across all different regions and seasons, with the maximum causality values rarely exceeding values over ± 0.25 . Since causality is a more stringent condition than correlation, as it requires a direct influence of one variable over another, more diffuse and weaker patterns suggest that the direct causal influence of these climate patterns on transmission potential is considerably more modest than simple correlation analysis would suggest. Additionally, since patterns are more spatially fragmented overall, direct causal climate influences on R_0 seem to operate through more localized mechanisms, instead of the more broader-scale patterns that correlation analyses might imply.

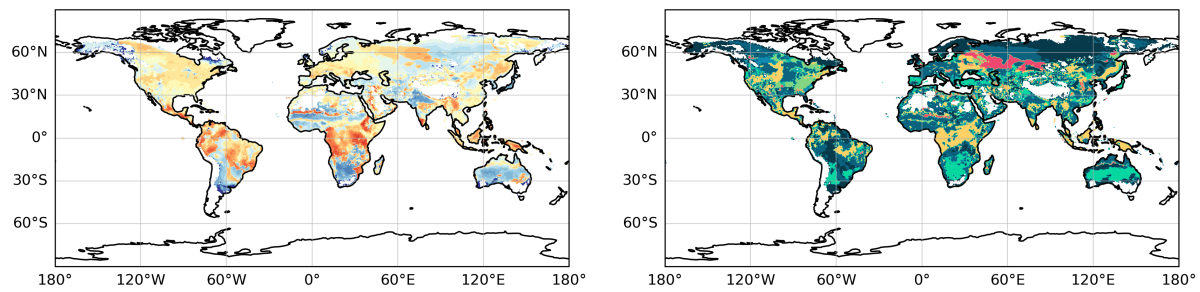
a) DJF



b) MAM



c) JJA



d) SON

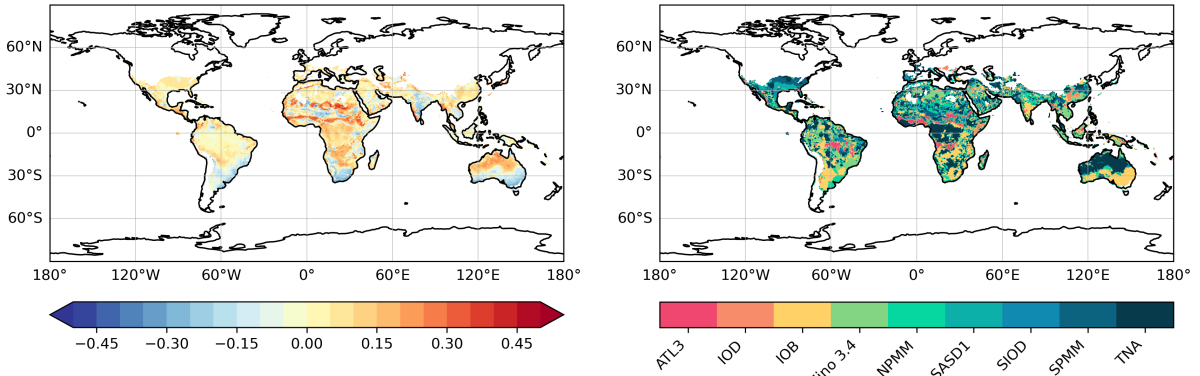


Figure 6. a)-d) For all seasons: Left, maximum statistically significant causality values between R_0 and all indexes of Table 1, for the 1951-2024 monthly mean period ($p < 0.01$). Right, which index gives the maximum statistically significant causality values.

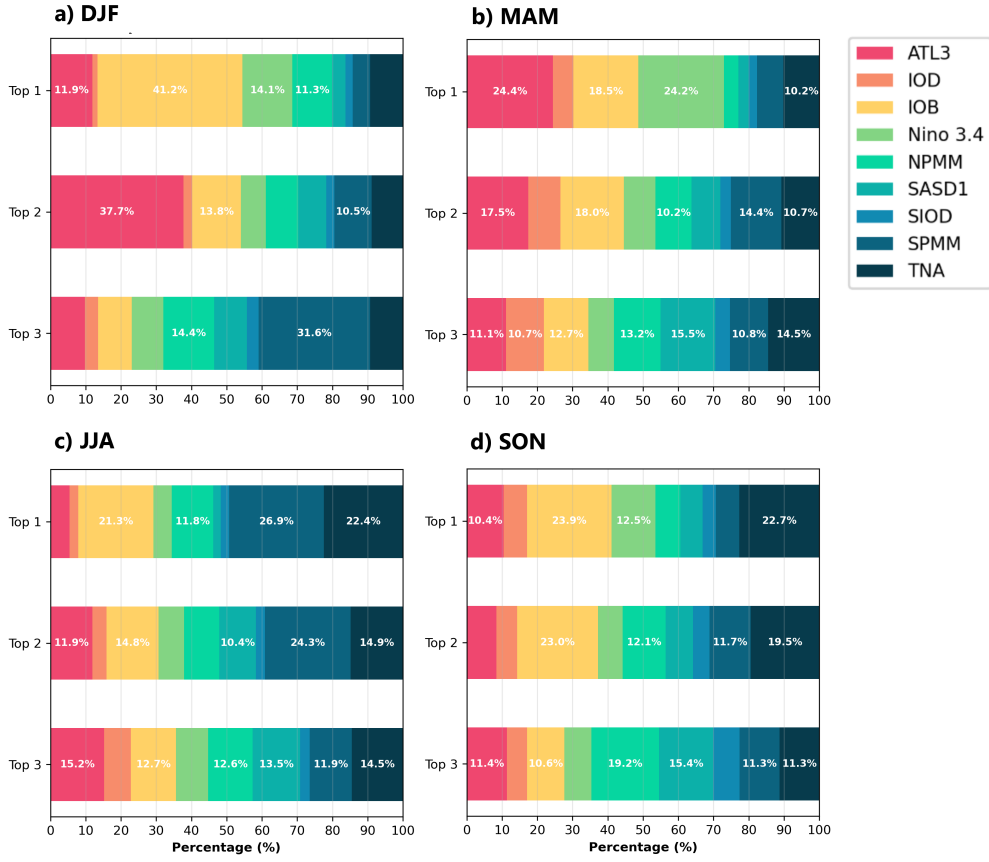


Figure 7. a)-d) For all seasons: Percentage of grid points over which each index gives the highest, second or third highest statistically significant causality values. Any contribution above 10% is labeled in the barplots.

Nonetheless, the causality analysis still provides valuable insights into the relationships between R_0 and climate variability indices. Positive Liang-Kleeman causality indicates that variations in any given climate pattern tend to amplify or destabilize fluctuations over R_0 (either favorably or unfavorably), leading to large changes in transmission potential. Alternatively, negative causality values suggest that variations in the climate index tend to dampen or stabilize fluctuations over R_0 , acting as a regulator for disease transmission and bringing R_0 toward more moderate values.

In this context, similarly to the correlation analyses, both the El Niño 3.4 index and IOB index are the most dominant causal indices over the austral summer and autumn months over the Amazon basin, central Africa and southeastern regions of Asia (Figure 6a-b), with other indices gaining prominence in these regions during the austral winter and spring months (Figure 6c-d). El Niño 3.4 shows negative causality values over all seasons (causal and stable). Along with the IOB index showing negative causality values over the spring and autumn months (Figure 6b, d), both of these climate patterns play a buffering effect, preventing extreme deviations on disease transmission values. On the other hand however, the IOB index shows positive causality values over

the summer and winter months (causal but unstable, 6a, c), aligning with the seasonal maximum and minimum of the pattern. It is during these months of peak DENV transmission in both hemispheres that this climate pattern pushes already marginal transmission conditions toward more extreme states: either making cold regions less suitable for transmission, or amplifying transmission windows in suitable or unsuitable areas.

The influence of both El Niño 3.4 and IOB indices on R_0 is through causality relationships can be seen in 7. While both indices do show a sizeable contribution over all categories, similarly to correlation, there is no clear dominance of any index during any season, with the second and third highest causality values being relatively evenly distributed across the different indices. Still, a notable shift occurs during boreal autumn and spring months (7b, d), with ATL3 gaining increased prominence while maintaining the multi-index influence pattern. The NPMM and SASD1 indices maintain substantial influence, while other indices show varying degrees of contribution. All of these ocean-based patterns show varying degrees of influence across regions with high seasonality (6b, d), suggesting that ocean basins become drivers of transmission variability at different times of the

year in these areas.

5 Discussion

- 5.1 The added value of climate patterns in seasonal forecasting of *Aedes*-borne diseases
- 5.2 Analysis 1: Multi-timescale climate decomposition of R_0
- 5.3 Analyses 2 and 3: Correlation and causality studies between R_0 and climate variability indices
- 5.4 Notable limitations and constraints

6 Conclusions

1. Historical and climatological analyses of R_0 values for *Aedes*-borne diseases provide insight in understanding the role of climate in disease emergence, and can be used to improve the accuracy of seasonal forecasts through the identification of climate predictors. However, while global climate models are suitable for a broad, general-purpose understanding, high-resolution data is preferred when more nuanced analysis are performed in endemic regions, in order to provide more accurate and actionable information for public health officials.

2.

7 Additional files

8 Abbreviations

- AeDES2: *Aedes Disease Environmental Suitability* 2
- AIC: Akaike Information Criterion
- ATL3: Atlantic 3 Index
- CHIKV: Chikungunya
- DENV: Dengue
- ENSO: El Niño Southern Oscillation
- GCV: Generalized cross-validation
- IOB: Indian Ocean Basin
- IOD: Indian Ocean Dipole
- LOESS: Locally estimated scatterplot smoothing
- NPMM: North Pacific Meridional Mode
- R^2 : Coefficient of determination
- SASD: South Atlantic Subtropical Dipole
- SIOD: Southern Indian Ocean Dipole
- SPMM: South Pacific Meridional Mode
- TNA: Tropical North Atlantic

- VBDs: Vector-borne diseases
- WHO: World Health Organization
- ZIKV: Zika

9 Acknowledgements

10 Funding

11 Availability of data and materials

Code for the generation of R_0 values employed for this study, computed using AeDES2's monitoring system, is available under request, and its values can be visualized in an operational, in-development Shiny App ([link](#)) for any region and grid-point. Additionally, the necessary datasets, functions and scripts to generate the maps and plots for this manuscript and supplementary material are available under the following GitHub repository: https://github.com/jacorvillo/monitoring_system_analysis

12 Authors' contributions

Á.M., V.T. and D.C. conceived the methodology to be undertaken in this manuscript. Data sources, code and figures were obtained and developed from the ground up by J.C, who also analysed the results. All authors have reviewed the manuscript.

13 Ethics approval and consent to participate

Not applicable.

14 Consent for publication

Not applicable.

15 Competing interests

The authors declare no competing interests.

16 Author details

17 References

References

1. Thomson, M. C., Garcia-Herrera, R. & Beniston, M. (eds.) *Seasonal Forecasts, Climatic Change and Human Health* (Springer Netherlands, Dordrecht, 2008).
2. Malloy, S. S., Horack, J. M., Lee, J. & Newton, E. K. Earth observation for public health: Biodiversity change and emerging disease surveillance. *Acta Astronaut.* **160**, 433–441, DOI: [10.1016/j.actaastro.2018.10.042](https://doi.org/10.1016/j.actaastro.2018.10.042) (2019).

3. Li, Y. *et al.* Global patterns in monthly activity of influenza virus, respiratory syncytial virus, parainfluenza virus, and metapneumovirus: A systematic analysis. *The Lancet. Glob. Heal.* **7**, e1031–e1045, DOI: [10.1016/S2214-109X\(19\)30264-5](https://doi.org/10.1016/S2214-109X(19)30264-5) (2019).
4. Shaman, J., Goldstein, E. & Lipsitch, M. Absolute humidity and pandemic versus epidemic influenza. *Am. J. Epidemiol.* **173**, 127–135, DOI: [10.1093/aje/kwq347](https://doi.org/10.1093/aje/kwq347) (2011).
5. Romero Starke, K. *et al.* The Effect of Ambient Environmental Conditions on COVID-19 Mortality: A Systematic Review. *Int. J. Environ. Res. Public Heal.* **18**, 6665, DOI: [10.3390/ijerph18126665](https://doi.org/10.3390/ijerph18126665) (2021).
6. Lowe, R. *et al.* Nonlinear and delayed impacts of climate on dengue risk in Barbados: A modelling study. *PLOS Medicine* **15**, e1002613, DOI: [10.1371/journal.pmed.1002613](https://doi.org/10.1371/journal.pmed.1002613) (2018).
7. Messina, J. P. *et al.* Mapping global environmental suitability for Zika virus. *eLife* **5**, e15272, DOI: [10.7554/eLife.15272](https://doi.org/10.7554/eLife.15272) (2016).
8. Campbell-Lendrum, D., Manga, L., Bagayoko, M. & Sommerfeld, J. Climate change and vector-borne diseases: What are the implications for public health research and policy? *Philos. Transactions Royal Soc. B: Biol. Sci.* **370**, 20130552, DOI: [10.1098/rstb.2013.0552](https://doi.org/10.1098/rstb.2013.0552) (2015).
9. Global Strategy for dengue prevention and control, 2012–2020. <https://www.who.int/publications/item/9789241504034>.
10. Yang, X., Quam, M. B. M., Zhang, T. & Sang, S. Global burden for dengue and the evolving pattern in the past 30 years. *J. Travel. Medicine* **28**, taab146, DOI: [10.1093/jtm/taab146](https://doi.org/10.1093/jtm/taab146) (2021).
11. Shepard, D. S., Coudeville, L., Halasa, Y. A., Zambrano, B. & Dayan, G. H. Economic Impact of Dengue Illness in the Americas. *The Am. J. Trop. Medicine Hyg.* **84**, 200–207, DOI: [10.4269/ajtmh.2011.10-0503](https://doi.org/10.4269/ajtmh.2011.10-0503) (2011).
12. Quam, M. B. *et al.* Estimating Air Travel–Associated Importations of Dengue Virus Into Italy. *J. Travel. Medicine* **22**, 186–193, DOI: [10.1111/jtm.12192](https://doi.org/10.1111/jtm.12192) (2015).
13. Lee, S. A., Economou, T., de Castro Catão, R., Barcellos, C. & Lowe, R. The impact of climate suitability, urbanisation, and connectivity on the expansion of dengue in 21st century Brazil. *PLoS neglected tropical diseases* **15**, e0009773, DOI: [10.1371/journal.pntd.0009773](https://doi.org/10.1371/journal.pntd.0009773) (2021).
14. Struchiner, C. J., Rocklöv, J., Wilder-Smith, A. & Massad, E. Increasing Dengue Incidence in Singapore over the Past 40 Years: Population Growth, Climate and Mobility. *PLOS ONE* **10**, e0136286, DOI: [10.1371/journal.pone.0136286](https://doi.org/10.1371/journal.pone.0136286) (2015).
15. Kraemer, M. U. *et al.* The global distribution of the arbovirus vectors Aedes aegypti and Ae. albopictus. *eLife* **4**, e08347, DOI: [10.7554/eLife.08347](https://doi.org/10.7554/eLife.08347) (2015).
16. Franklinos, L. H. V., Jones, K. E., Redding, D. W. & Abubakar, I. The effect of global change on mosquito-borne disease. *The Lancet Infect. Dis.* **19**, e302–e312, DOI: [10.1016/S1473-3099\(19\)30161-6](https://doi.org/10.1016/S1473-3099(19)30161-6) (2019).
17. Ooi, E.-E. & Gubler, D. J. Dengue in Southeast Asia: Epidemiological characteristics and strategic challenges in disease prevention. *Cadernos de Saúde Pública* **25**, S115–S124, DOI: [10.1590/S0102-311X2009001300011](https://doi.org/10.1590/S0102-311X2009001300011) (2009).
18. Dengue - Annual Epidemiological Report for 2022. <https://www.ecdc.europa.eu/en/publications-data/dengue-annual-epidemiological-report-2022> (2024).
19. Nakase, T., Giovanetti, M., Obolski, U. & Lourenço, J. Population at risk of dengue virus transmission has increased due to coupled climate factors and population growth. *Commun. Earth & Environ.* **5**, 1–11, DOI: [10.1038/s43247-024-01639-6](https://doi.org/10.1038/s43247-024-01639-6) (2024).
20. Pourzangiabadi, M., Najafi, H., Fallah, A., Goudarzi, A. & Pouladi, I. Dengue virus: Etiology, epidemiology, pathobiology, and developments in diagnosis and control – A comprehensive review. *Infect. Genet. Evol.* **127**, 105710, DOI: [10.1016/j.meegid.2024.105710](https://doi.org/10.1016/j.meegid.2024.105710) (2025).
21. Mordecai, E. A. *et al.* Thermal biology of mosquito-borne disease. *Ecol. Lett.* **22**, 1690–1708, DOI: [10.1111/ele.13335](https://doi.org/10.1111/ele.13335) (2019).
22. Paaijmans, K. P., Wandago, M. O., Githeko, A. K. & Takken, W. Unexpected High Losses of Anopheles gambiae Larvae Due to Rainfall. *PLOS ONE* **2**, e1146, DOI: [10.1371/journal.pone.0001146](https://doi.org/10.1371/journal.pone.0001146) (2007).
23. Colón-González, F. J. *et al.* Projecting the risk of mosquito-borne diseases in a warmer and more populated world: A multi-model, multi-scenario intercomparison modelling study. *The Lancet Planet. Heal.* **5**, e404–e414, DOI: [10.1016/S2542-5196\(21\)00132-7](https://doi.org/10.1016/S2542-5196(21)00132-7) (2021).
24. Descloux, E. *et al.* Climate-Based Models for Understanding and Forecasting Dengue Epidemics. *PLOS Neglected Trop. Dis.* **6**, e1470, DOI: [10.1371/journal.pntd.0001470](https://doi.org/10.1371/journal.pntd.0001470) (2012).
25. Caminade, C. *et al.* Global risk model for vector-borne transmission of Zika virus reveals the role of El Niño 2015. *Proc. Natl. Acad. Sci.* **114**, 119–124, DOI: [10.1073/pnas.1614303114](https://doi.org/10.1073/pnas.1614303114) (2017).
26. Liu-Helmersson, J., Stenlund, H., Wilder-Smith, A. & Rocklöv, J. Vectorial Capacity of Aedes aegypti: Effects of Temperature and Implications for Global Dengue Epidemic Potential. *PLOS ONE* **9**, e89783, DOI: [10.1371/journal.pone.0089783](https://doi.org/10.1371/journal.pone.0089783) (2014).

- 27.** Mordecai, E. A. *et al.* Detecting the impact of temperature on transmission of Zika, dengue, and chikungunya using mechanistic models. *PLOS Neglected Trop. Dis.* **11**, e0005568, DOI: [10.1371/journal.pntd.0005568](https://doi.org/10.1371/journal.pntd.0005568) (2017).
- 28.** Wesolowski, A. *et al.* Impact of human mobility on the emergence of dengue epidemics in Pakistan. *Proc. Natl. Acad. Sci.* **112**, 11887–11892, DOI: [10.1073/pnas.1504964112](https://doi.org/10.1073/pnas.1504964112) (2015).
- 29.** Erraguntla, M. *et al.* Predictive model for microclimatic temperature and its use in mosquito population modeling. *Sci. Reports* **11**, 18909, DOI: [10.1038/s41598-021-98316-x](https://doi.org/10.1038/s41598-021-98316-x) (2021).
- 30.** Lee, H. S. *et al.* Seasonal patterns of dengue fever and associated climate factors in 4 provinces in Vietnam from 1994 to 2013. *BMC Infect. Dis.* **17**, 218, DOI: [10.1186/s12879-017-2326-8](https://doi.org/10.1186/s12879-017-2326-8) (2017).
- 31.** Yavari Nejad, F. & Varathan, K. D. Identification of significant climatic risk factors and machine learning models in dengue outbreak prediction. *BMC Med. Informatics Decis. Mak.* **21**, 141, DOI: [10.1186/s12911-021-01493-y](https://doi.org/10.1186/s12911-021-01493-y) (2021).
- 32.** Sriklin, T., Kajornkasirat, S. & Puttinaovarat, S. Dengue Transmission Mapping with Weather-Based Predictive Model in Three Southernmost Provinces of Thailand. *Sustainability* **13**, 6754, DOI: [10.3390/su13126754](https://doi.org/10.3390/su13126754) (2021).
- 33.** Ali, H. & Charles, H. Mosquito Breeding Hotspots in a Changing World: Remote Sensing and GIS-Based Analysis of Ecological and Anthropogenic Factors. Tech. Rep. (2025). DOI: [10.13140/RG.2.2.29354.94406](https://doi.org/10.13140/RG.2.2.29354.94406).
- 34.** Shaw, T. A. *et al.* Regional climate change: Consensus, discrepancies, and ways forward. *Front. Clim.* **6**, DOI: [10.3389/fclim.2024.1391634](https://doi.org/10.3389/fclim.2024.1391634) (2024).
- 35.** Sen Roy, S. Climate Change in the Global South: Trends and Spatial Patterns. In Sen Roy, S. (ed.) *Linking Gender to Climate Change Impacts in the Global South*, 1–25, DOI: [10.1007/978-3-319-75777-3_1](https://doi.org/10.1007/978-3-319-75777-3_1) (Springer International Publishing, Cham, 2018).
- 36.** Peng, C., Zeng, J., Chen, K.-S., Ma, H. & Bi, H. Spatiotemporal Patterns and Influencing Factors Of Soil Moisture At A Global Scale. In *IGARSS 2023 - 2023 IEEE International Geoscience and Remote Sensing Symposium*, 3174–3177, DOI: [10.1109/IGARSS52108.2023.10282096](https://doi.org/10.1109/IGARSS52108.2023.10282096) (2023).
- 37.** Lübbecke, J. F. *et al.* Equatorial Atlantic variability—Modes, mechanisms, and global teleconnections. *WIREs Clim. Chang.* **9**, e527, DOI: [10.1002/wcc.527](https://doi.org/10.1002/wcc.527) (2018).
- 38.** Lee, D., Ward, P. & Block, P. Attribution of Large-Scale Climate Patterns to Seasonal Peak-Flow and Prospects for Prediction Globally. *Water Resour. Res.* **54**, 916–938, DOI: [10.1002/2017WR021205](https://doi.org/10.1002/2017WR021205) (2018).
- 39.** Easterbrook, D. J. Chapter 21 - Using Patterns of Recurring Climate Cycles to Predict Future Climate Changes. In Easterbrook, D. J. (ed.) *Evidence-Based Climate Science (Second Edition)*, 395–411, DOI: [10.1016/B978-0-12-804588-6.00021-5](https://doi.org/10.1016/B978-0-12-804588-6.00021-5) (Elsevier, 2016).
- 40.** Hallett, T. B. *et al.* Why large-scale climate indices seem to predict ecological processes better than local weather. *Nature* **430**, 71–75, DOI: [10.1038/nature02708](https://doi.org/10.1038/nature02708) (2004).
- 41.** Keating, C. *Tore Godal and the Evolution of Global Health* (Routledge, New York, 2023), 1 edn.
- 42.** Ramirez, B. & TDR-IDRC Research Initiative on Vector Borne Diseases and Climate Change. Support for research towards understanding the population health vulnerabilities to vector-borne diseases: Increasing resilience under climate change conditions in Africa. *Infect. Dis. Poverty* **6**, 164, DOI: [10.1186/s40249-017-0378-z](https://doi.org/10.1186/s40249-017-0378-z) (2017).
- 43.** Muñoz, Á. G. *et al.* AeDES: A next-generation monitoring and forecasting system for environmental suitability of Aedes-borne disease transmission. *Sci. Reports* **10**, 12640, DOI: [10.1038/s41598-020-69625-4](https://doi.org/10.1038/s41598-020-69625-4) (2020).
- 44.** Guerra, J. C. *et al.* From climate variables to health information - Predicting and monitoring mosquito-borne disease outbreaks with AeDES2. Tech. Rep. EGU25-15204, Copernicus Meetings (2025). DOI: [10.5194/egusphere-egu25-15204](https://doi.org/10.5194/egusphere-egu25-15204).
- 45.** Leandro, A. & Maciel-de-Freitas, R. Development of an Integrated Surveillance System to Improve Preparedness for Arbovirus Outbreaks in a Dengue Endemic Setting: Descriptive Study. *JMIR Public Heal. Surveillance* **10**, e62759, DOI: [10.2196/62759](https://doi.org/10.2196/62759) (2024).
- 46.** Ropelewski, C. F., Janowiak, J. E. & Halpert, M. S. The Analysis and Display of Real Time Surface Climate Data. *Mon. Weather. Rev.* **113**, 1101–1106, DOI: [10.1175/1520-0493\(1985\)113<1101:TAADOR>2.0.CO;2](https://doi.org/10.1175/1520-0493(1985)113<1101:TAADOR>2.0.CO;2) (1985).
- 47.** Thomson, M. C. *et al.* Malaria early warnings based on seasonal climate forecasts from multi-model ensembles. *Nature* **439**, 576–579, DOI: [10.1038/nature04503](https://doi.org/10.1038/nature04503) (2006).
- 48.** (PDF) Detecting Epidemic Malaria, Uganda. *ResearchGate* DOI: [10.3201/eid1305.061410](https://doi.org/10.3201/eid1305.061410).
- 49.** Moriyama, M., Hugentobler, W. J. & Iwasaki, A. Seasonality of Respiratory Viral Infections. *Annu. Rev. Virol.* **7**, 83–101, DOI: [10.1146/annrev-virology-012420-022445](https://doi.org/10.1146/annrev-virology-012420-022445) (2020).
- 50.** Dietz, K. The estimation of the basic reproduction number for infectious diseases. *Stat. Methods Med. Res.* **2**, 23–41, DOI: [10.1177/096228029300200103](https://doi.org/10.1177/096228029300200103) (1993).
- 51.** WHO guidance for surveillance during an influenza pandemic, 2017 update. <https://www.who.int/publications/i/item/9789241513333>.
- 52.** Chiew, M. *et al.* Estimating the measles effective reproduction number in Australia from routine notification data. *Bull. World Heal. Organ.* **92**, 171–177, DOI: [10.2471/BLT.13.125724](https://doi.org/10.2471/BLT.13.125724) (2014).

- 53.** Thomson, M. C., Muñoz, Á. G., Cousin, R. & Shumake-Guillemot, J. Climate drivers of vector-borne diseases in Africa and their relevance to control programmes. *Infect. Dis. Poverty* **7**, 81, DOI: [10.1186/s40249-018-0460-1](https://doi.org/10.1186/s40249-018-0460-1) (2018).
- 54.** Muñoz, Á. G., Thomson, M. C., Goddard, L. & Aldighieri, S. Analyzing climate variations at multiple timescales can guide Zika virus response measures. *GigaScience* **5**, 41, DOI: [10.1186/s13742-016-0146-1](https://doi.org/10.1186/s13742-016-0146-1) (2016).
- 55.** Jacoby, W. G. Loess:: A nonparametric, graphical tool for depicting relationships between variables. *Elect. Stud.* **19**, 577–613, DOI: [10.1016/S0261-3794\(99\)00028-1](https://doi.org/10.1016/S0261-3794(99)00028-1) (2000).
- 56.** Craven, P. & Wahba, G. Smoothing noisy data with spline functions. *Numer. Math.* **31**, 377–403, DOI: [10.1007/BF01404567](https://doi.org/10.1007/BF01404567) (1978).
- 57.** Marcotte, D. Generalized cross-validation for covariance model selection. *Math. Geol.* **27**, 659–672, DOI: [10.1007/BF02093906](https://doi.org/10.1007/BF02093906) (1995).
- 58.** Fan, Y. & van den Dool, H. A global monthly land surface air temperature analysis for 1948–present. *J. Geophys. Res. Atmospheres* **113**, DOI: [10.1029/2007JD008470](https://doi.org/10.1029/2007JD008470) (2008).
- 59.** Xie, P., Arkin, P. A. & Janowiak, J. E. CMAP: The CPC Merged Analysis of Precipitation. In Levizzani, V., Bauer, P. & Turk, F. J. (eds.) *Measuring Precipitation From Space: EURAINSAT and the Future*, 319–328, DOI: [10.1007/978-1-4020-5835-6_25](https://doi.org/10.1007/978-1-4020-5835-6_25) (Springer Netherlands, Dordrecht, 2007).
- 60.** Chen, M. *et al.* Assessing objective techniques for gauge-based analyses of global daily precipitation. *J. Geophys. Res. Atmospheres* **113**, DOI: [10.1029/2007JD009132](https://doi.org/10.1029/2007JD009132) (2008).
- 61.** (PDF) Web tool deconstructs variability in twentieth-century climate. *ResearchGate* DOI: [10.1029/2011EO450001](https://doi.org/10.1029/2011EO450001).
- 62.** Spearman, C. The Proof and Measurement of Association between Two Things. *The Am. J. Psychol.* **15**, 72–101, DOI: [10.2307/1412159](https://doi.org/10.2307/1412159) (1904). [1412159](#).
- 63.** New, M. & Hulme, M. Representing uncertainty in climate change scenarios: A Monte-Carlo approach. *Integr. Assess.* **1**, 203–213, DOI: [10.1023/A:1019144202120](https://doi.org/10.1023/A:1019144202120) (2000).
- 64.** Liang, X. S. Unraveling the cause-effect relation between time series. *Phys. Rev. E* **90**, 052150, DOI: [10.1103/PhysRevE.90.052150](https://doi.org/10.1103/PhysRevE.90.052150) (2014).
- 65.** Liang, X. S. Normalizing the causality between time series. *Phys. Rev. E* **92**, 022126, DOI: [10.1103/PhysRevE.92.022126](https://doi.org/10.1103/PhysRevE.92.022126) (2015).
- 66.** Beck, H. E. *et al.* High-resolution (1 km) Köppen-Geiger maps for 1901–2099 based on constrained CMIP6 projections. *Sci. Data* **10**, 724, DOI: [10.1038/s41597-023-02549-6](https://doi.org/10.1038/s41597-023-02549-6) (2023).
- 67.** Triantafyllou, G. N. & Tsonis, A. A. Assessing the ability of the Köppen System to delineate the general world pattern of climates. *Geophys. Res. Lett.* **21**, 2809–2812, DOI: [10.1029/94GL01992](https://doi.org/10.1029/94GL01992) (1994).
- 68.** Chen, Y. *et al.* Indian Ocean temperature anomalies predict long-term global dengue trends. *Science* **384**, 639–646, DOI: [10.1126/science.adj4427](https://doi.org/10.1126/science.adj4427) (2024).
- 69.** Kurnianingsih, Wirasatriya, A., Lazuardi, L., Kubota, N. & Ng, N. IOD and ENSO-Related Time Series Variability and Forecasting of Dengue and Malaria Incidence in Indonesia. In *2020 International Symposium on Community-centric Systems (CcS)*, 1–8, DOI: [10.1109/CcS49175.2020.9231358](https://doi.org/10.1109/CcS49175.2020.9231358) (2020).
- 70.** Banu, S. *et al.* Impacts Of El Niño Southern Oscillation And Indian Ocean Dipole On Dengue Incidence In Bangladesh. *ISEE Conf. Abstr.* **2015**, 746, DOI: [10.1289/isee.2015.2015-746](https://doi.org/10.1289/isee.2015.2015-746) (2015).